

# Two-dimensional homography-based correction of positional errors in widefield MRT images

Arvind Nayak,<sup>1\*</sup> Soobash Daiboo<sup>1,2</sup> and N. Udaya Shankar<sup>1</sup>

<sup>1</sup>*Raman Research Institute, C.V. Raman Avenue, Sadashivanagar, Bangalore 560 080, India*

<sup>2</sup>*Physics Department, University of Mauritius, Reduit, Mauritius*

Accepted 2010 June 09. Received 2010 June 04; in original form 2010 February 02

## ABSTRACT

A steradian of the southern sky has been imaged at 151.5 MHz using the Mauritius Radio Telescope (MRT). These images show systematics in positional errors of sources when compared to source positions in the Molonglo Reference Catalogue (MRC). We have applied two-dimensional homography to correct for systematic positional errors in the image domain and thereby avoid re-processing the visibility data. Positions of bright (above  $15\text{-}\sigma$ ) point sources, common to MRT catalogue and MRC, are used to set up an over-determined system to solve for the homography matrix. After correction the errors are found to be within 10% of the beamwidth for these bright sources and the systematics are eliminated from the images. This technique will be of relevance to the new generation radio telescopes where, owing to huge data rates, only images after a certain integration would be recorded as opposed to raw visibilities. It is also interesting to note how our investigations cued to possible errors in the array geometry. The analysis of positional errors of sources showed that MRT images are stretched in declination by  $\sim 1$  part in 1000. This translates to a compression of the baseline scale in the visibility domain. The array geometry was re-estimated using the astrometry principle. The estimates show an error of  $\sim 1$  mm/m, which results in an error of about half a wavelength at 150 MHz for a 1 km north-south baseline. The estimates also indicate that the east-west arm is inclined by an angle of  $\sim 40''$  to the true east-west direction.

**Key words:** surveys – techniques: image processing – astrometry – techniques: interferometric – telescope – catalogues

## 1 INTRODUCTION

The Mauritius Radio Telescope (MRT) (Golap et al. 1995a; Udaya Shankar et al. 2002) is a Fourier synthesis, T-shaped non-coplanar array operating at 151.5 MHz. The telescope was built to fill the gap in the availability of deep sky surveys at low radio frequencies in the southern hemisphere. The aim of the survey with MRT is to contribute to the database of southern sky sources in the declination ( $\delta$ ) range  $-70^\circ$  to  $-10^\circ$ , covering the entire right ascension ( $\alpha$ ), with a synthesised beam of  $4' \times 4'.6 \text{ sec } za$  and an expected point source sensitivity ( $1\text{-}\sigma$ ) of  $\sim 110 \text{ mJy beam}^{-1}$ . The *zenith angle* ( $za$ ) is given by  $(\delta - \phi)$ , where,  $\phi$  ( $\approx -20.14^\circ$ ) is the latitude of MRT. MRT has been designed to be the southern-sky equivalent of the Cambridge 6C survey at 151.5 MHz (Baldwin et al. 1985).

The next generation radio telescopes, like the LOw Frequency ARray (LOFAR) and the Murchison Widefield Ar-

ray (MWA), that are being built are low frequency arrays; clearly indicating a renewed interest in metre-wavelength astronomy. The key astrophysical science drivers include acceleration, turbulence and propagation in the galactic interstellar medium, exploring the high redshift universe and transient phenomenon, as well as searching for the redshifted signature of neutral hydrogen from the cosmologically important epoch of reionisation (EoR). The surveys made using such arrays will provide critical information about foregrounds which will also provide a useful database for both extragalactic and galactic sources. MRT survey at 151.5 MHz is a step in that direction and, in addition, will provide the crucial sky model for calibration.

Imaging at MRT is presently done only on the meridian to minimise the problems of non-coplanarity. A two-dimensional (2-D) image in  $\alpha\text{-sin } za$  coordinates is formed by stacking one-dimensional (1-D) images on the meridian at different sidereal times. Images of  $\sim$  a steradian ( $18^h \leq \alpha \leq 24^h, -70^\circ \leq \delta \leq -10^\circ$ ) of the southern sky, with an rms noise in images of  $\sim 300 \text{ mJy beam}^{-1}$  (1-

\* E-mail: arvind@rri.res.in

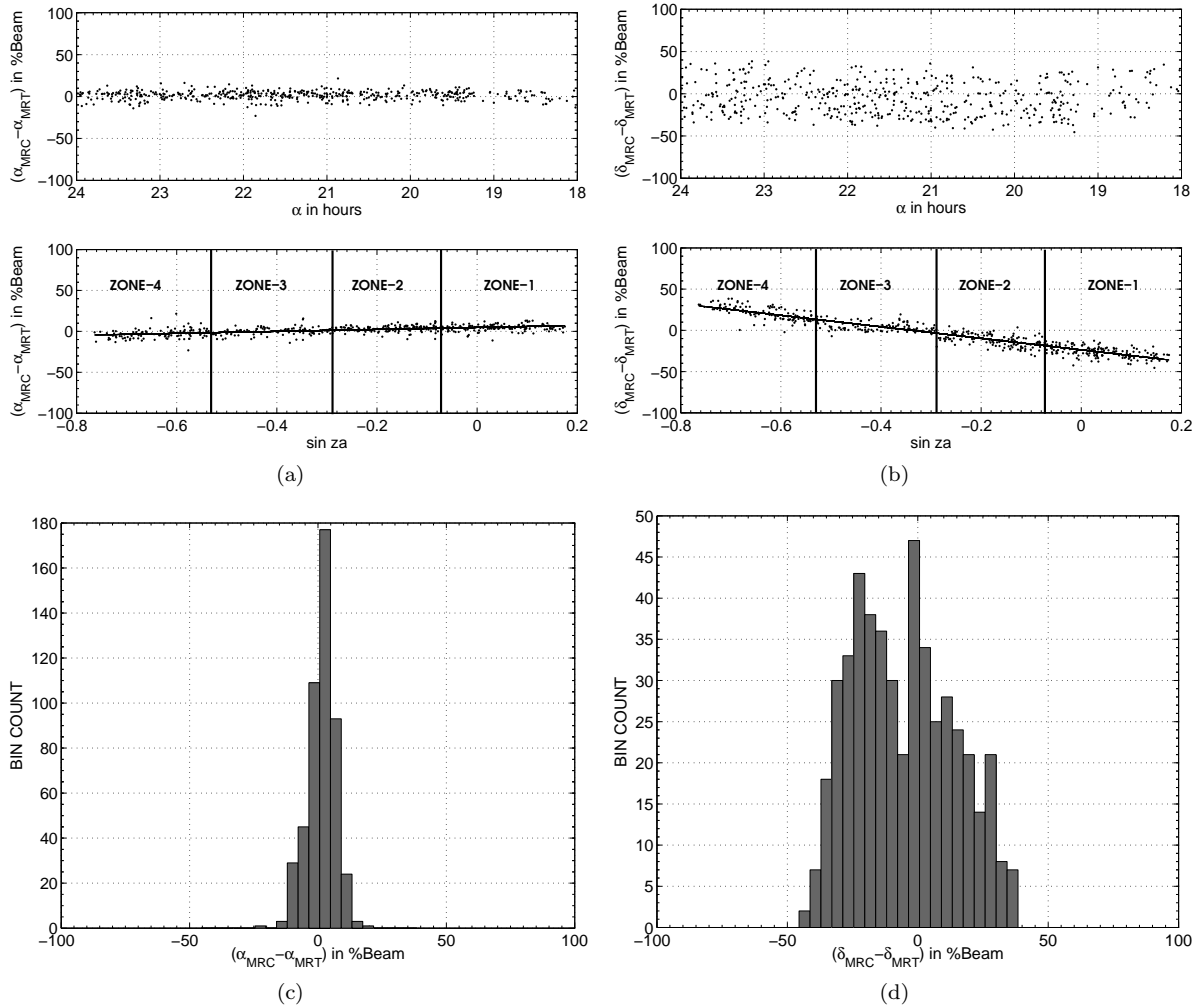


**Figure 1.** Positional error analysis of  $\sim 400$  sources (above  $15\text{-}\sigma$ ) common to MRT catalogue and MRC. For visualisation, the errors are shown in percentages of MRT beamwidths. **(a)** The *first row* subplot shows errors in  $\alpha$  against  $\alpha$ ; no systematics are observed. The *second row* subplot shows errors in  $\alpha$  against  $\sin za$ ; errors show a linear gradient as a function of  $\sin za$ . **(b)** The *first row* subplot shows errors in  $\delta$  against  $\alpha$ ; no systematics are observed. The *second row* subplot shows errors in  $\delta$  against  $\sin za$ ; errors show a linear gradient as a function of  $\sin za$ . The *second row* subplots in (a) and (b) also indicate declination (or equivalent  $\sin za$ ) ranges of the four zones imaged with different delay settings. **(c)** and **(d)** show histograms of errors in  $\alpha$  and  $\delta$ , respectively. The histogram of errors in  $\delta$  shows a broader spread compared to errors in  $\alpha$ .

$\sigma$ ), were produced by Pandey and Udaya Shankar (2005). A suite of programs developed in-house was used to reduce  $\sim 5000$  hours of the survey data (a quarter of the total  $\sim 20,000$  hours observed over a span of  $\sim 5$  years). The deconvolved images and a source catalogue of  $\sim 2,800$  sources were published by Pandey (2006).

Systematics in positional errors were found when the positions of sources common to MRT catalogue and the Molonglo Reference Catalogue (MRC) (Large et al. 1981) were compared. Pandey (2006) treated the systematics in errors in  $\alpha$  and  $\sin za$  independently. By estimating two separate 1-D least-squares fits for errors in  $\alpha$  and  $\sin za$  the systematics were corrected only in the source catalogue. However, errors remained in the images which impede usefulness of MRT images for multi-wavelength analysis of sources. In addition, the source of errors was not investigated. At MRT, the visibility data is processed through several complex stages of data reduction specific to the array, especially, arising due

to its non-coplanarity (Udaya Shankar et al. 2002). It was therefore decided to correct for errors in the image domain and avoid re-processing the visibility data.

This paper describes the application of 2-D homography, a technique ubiquitous in the computer vision and graphics community, to correct the errors in the image domain. Homography is used to estimate a transformation matrix (which includes rotation, translation and non-isotropic scaling) that accounts for positional errors in the linearly gridded 2-D images. In our view, this technique will be of relevance to the new generation radio telescopes where, owing to huge data rates, only images after a certain integration would be recorded as opposed to raw visibilities (Lonsdale et al. 2009). This paper also describes our investigations tracing the positional errors to errors in the array geometry used for imaging. Our hypothesis on the array geometry, its subsequent confirmation endorsed by re-

estimation of the array geometry and its effect on the images are also described.

The rest of the paper is organised as follows. Section 2 compares positions of sources common to MRT catalogue and MRC. The 2-D homography estimation is briefly described in Section 3. Section 4 presents the correction scheme and typical results. The re-estimation of MRT array geometry is described in Section 5. Finally, we summarise and present our conclusions in Section 6.

## 2 POSITIONAL ERRORS

The positions of sources common to MRT catalogue and MRC were compared. We used MRC because of its overlap with MRT survey, its proximity in frequency compared to other reliable catalogues available and, comparable resolution ( $2'.62 \times 2'.86 \text{ sec}(\delta + 35^\circ.5)$ ). Moreover, for sources of listed flux density  $\geq 1.00 \text{ Jy}$  (at 408 MHz) the catalogue is reported to be substantially complete and, the reliability is reported to be 99.9% (Large et al. 1981). For our further discussions, errors in MRC source positions are considered random, without any systematics.

About 400 bright sources common to the two catalogues and with flux density at 151.5 MHz greater than  $5 \text{ Jy}$  ( $> 15\sigma$ ) were identified and their positions were compared. The sources were labelled as common if they lie within  $4'$  of each other. Since MRC has a source density of  $\sim 0.5 \text{ source deg}^{-2}$ , the chances of considering two unrelated sources as common are extremely low. A flux threshold of  $15\sigma$  ensures a source population abundant to reliably estimate homography (explained in next section).

The positional errors in  $\alpha$  and  $\delta$  show no systematics as a function of  $\alpha$  (refer *first rows* of Fig. 1a and 1b). For visualisation, the errors are shown in percentages of MRT beamwidths. The errors in  $\alpha$  and  $\delta$  show a linear gradient as a function of  $\sin za$ . The errors in  $\alpha$ , plotted against  $\sin za$ , reach  $\sim \pm 10\%$  of the MRT beamwidth (refer *second row* of Fig. 1a). Whereas, the errors in  $\delta$ , plotted against  $\sin za$ , are significant and reach  $\sim \pm 50\%$  of MRT beamwidth. (refer *second row* of Fig. 1b). Histograms in Fig. 1c and Fig. 1d show the distribution of errors in  $\alpha$  and  $\delta$ , respectively. The histogram of errors in  $\delta$  shows a broader spread compared to errors in  $\alpha$ .

Re-imaging, to correct for errors in the images, would involve re-reducing the  $\sim 5,000$  hours of observed data. Owing to the complexity involved it was decided to correct for the positional errors in the images, thus avoiding re-processing. The 2-D homography estimation technique was employed for correcting positional errors in images and is discussed in detail in the following section.

## 3 2-D HOMOGRAPHY

The 2-D planar homography is a non-singular linear relationship between points on planes. Given two sets of  $K$  corresponding image points in projective coordinates,  $(\mathbf{p}_k \text{ and } \mathbf{p}'_k) \in \mathbb{P}^2$ , homography maps  $\mathbf{p}_k$  to the corresponding  $\mathbf{p}'_k$  (Hartley and Zisserman 2000). Where,  $k = 1, \dots, K$ . The homography sought here is a non-singular  $3 \times 3$  matrix

$\mathbf{H}$  such that:

$$\begin{bmatrix} x'_k \\ y'_k \\ 1 \end{bmatrix} = \begin{bmatrix} h_{11} & h_{12} & h_{13} \\ h_{21} & h_{22} & h_{23} \\ h_{31} & h_{32} & h_{33} \end{bmatrix} \begin{bmatrix} x_k \\ y_k \\ 1 \end{bmatrix}. \quad (1)$$

Where,  $(x_k, y_k)$  and  $(x'_k, y'_k)$  represent  $(\alpha, \sin za)$  of  $K$  corresponding MRT and MRC sources, respectively.

In Equation 1,  $(x_k, y_k, 1)$  and  $(x'_k, y'_k, 1)$  are referred to as the *homogeneous coordinates* and are always represented one dimension higher than the dimension of the problem space. This is a commonly used representation in computer graphics. The simple reason is that with a  $2 \times 2$  matrix one can only *rotate* a set of 2-D points around the origin and *scale* them towards or away from the origin. A  $2 \times 2$  matrix is incapable of *translating* a set of 2-D points. The homogeneous coordinates allow one to express a translation as a multiplication. A single  $3 \times 3$  matrix, with homogeneous coordinates, can account for rotation, scaling and translation of 2-D coordinates. For example, from Equation 1,  $x'_k = h_{11}x_k + h_{12}y_k + h_{13}$ . Notice,  $h_{13}$  (representing translation in  $\alpha$ -dimension) is simply being added to the normal dot product  $(h_{11}x_k + h_{12}y_k)$  that together represents rotation and scaling. In homogeneous coordinates, the 2-D problem space is a plane hovering in the third dimension at a unit distance.

A general homography matrix, for projective transformation, has 8 degrees-of-freedom (DOF). For our system, both errors in  $\alpha$  and  $\delta$  have only  $\sin za$ -dependency. Therefore, a less general, 2-D affine transformation is sufficient. A 2-D affine transformation (two rotations, two translations and two scalings) requires 6-DOF (Hartley and Zisserman 2000), therefore in  $\mathbf{H}$ ,  $h_{31}$  and  $h_{32}$  are zero. Since each 2-D point provides two independent equations, a minimum of 3 point correspondences are necessary to constrain  $\mathbf{H}$  in the affine space. A set of  $K$  such equation pairs, contributed by  $K$  point correspondences, form an over-determined linear system:

$$\mathbf{A}\mathbf{h} = \mathbf{b}, \text{ where,}$$

$$\mathbf{A} = \begin{bmatrix} x_1 & y_1 & 1 & 0 & 0 & 0 & -x_1x'_1 & -x'_1y_1 \\ 0 & 0 & 0 & x_1 & y_1 & 1 & -x_1y'_1 & -y_1y'_1 \\ \vdots & & & & & & & \vdots \\ x_K & y_K & 1 & 0 & 0 & 0 & -x_Kx'_K & -x'_Ky_K \\ 0 & 0 & 0 & x_K & y_K & 1 & -x_Ky'_K & -y_Ky'_K \end{bmatrix},$$

$$\mathbf{h} = [h_{11}, h_{12}, h_{13}, h_{21}, h_{22}, h_{23}, h_{31}, h_{32}]^T \text{ and,}$$

$$\mathbf{b} = [x'_1, y'_1, \dots, x'_K, y'_K]^T. \quad (2)$$

In Equation 2,  $T$  represents transpose of a matrix. This system can be solved by least squares-based estimators.

At this stage it is useful to consider the effect of using  $(\alpha, \sin za)$ -coordinates to represent the brightness distribution on the celestial sphere. Ideally, it is the directional cosines  $(l, m, n)$ , with respect to the coordinates of the array, which represent the spherical coordinates in the sky. Therefore, the image coordinates in which homography should in principle be estimated are  $(l, m)$ . However, at MRT, for 1-D imaging on the meridian:

$$m = \sin za. \quad (3)$$

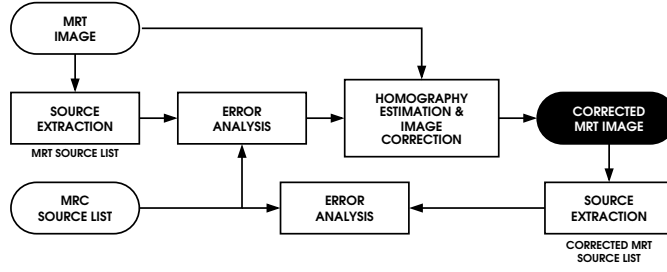


**Figure 2.** Block schematic of the correction scheme. Rectangular boxes represent processes; rounded boxes, data or results.

Therefore,  $\sin za$  is a natural choice for one of the coordinates and is indeed used in the present case. On the meridian, the directional cosine  $l$  is zero. For small errors,  $\Delta l$ , in  $l$ , i.e. close to the meridian:

$$\Delta l = \cos \delta \Delta \alpha. \quad (4a)$$

$$\therefore \Delta \alpha = \Delta l \sec \delta. \quad (4b)$$

Here,  $\Delta \alpha$  is the error in  $\alpha$ . Equation 4 shows that an error in  $l$  will lead to an error in  $\alpha$  with a  $\sec \delta$ -dependence.

The 2-D images of MRT are 1-D images on the meridian made at different sidereal times and stacked. Therefore, positional errors both in  $\alpha$  and  $\delta$  do not show systematics as a function of  $\alpha$  (*first rows* of Figs. 1a and 1b). We preferred  $(\alpha, \sin za)$ -representation because all MRT images were already generated in this coordinate system. This choice compelled us to seek solutions for errors in  $\alpha$  as a function of  $\sin za$  rather than  $\sec \delta$ . We plotted errors in  $\alpha$  against both  $\sec \delta$  and  $\sin za$  and obtained separate linear least-squares fits. The rms of residuals in both fits is  $\sim 5\%$  of the beamwidth in  $\alpha$ . However, the rms of difference between the fitting functions  $\sec \delta$  and  $\sin za$  in the  $\delta$  range of MRT ( $-70^\circ$  to  $-10^\circ$ ) is only  $\sim 1.5\%$  of the beamwidth in  $\alpha$ . Therefore, the random errors in the source positions are larger than the errors introduced by the preferred  $(\alpha, \sin za)$ -coordinates for  $\mathbf{p}_k$  and  $\mathbf{p}'_k$ .

In  $\mathbf{p}_k$  and  $\mathbf{p}'_k$ , the  $\alpha$  ranges from 18 hours to 24 hours and the  $\sin za$  ranges from  $-0.8$  to  $0.2$  (corresponding to the declination range of  $-70^\circ$  to  $-10^\circ$ ). Moreover, in matrix  $\mathbf{A}$  (refer Equation 2) there are entries of 1's & 0's. Such a matrix is ill-conditioned and in the presence of noise in the source positions, the solution for an over-determined system may diverge from the correct estimate (Hartley and Zisserman 2000). The effect of an ill-conditioned matrix is that it amplifies the divergence. A normalisation (or pre-conditioning) is therefore required.

### 3.1 Data normalisation and denormalisation

To obtain a good estimate of the transformation matrix we adopted the normalisation scheme proposed by Hartley (1997). The normalisation ensures freedom on arbitrary choices of scale and coordinate origin, leading to algebraic minimisation in a fixed canonical frame. The homography matrix  $\tilde{\mathbf{H}}$  is estimated from normalised coordinates by the least-squares method using singular value decomposition (SVD). The matrix is then denormalised to obtain  $\mathbf{H}$ . The scheme is briefly described below:

(i) **Normalisation of  $\mathbf{p}$ :** Compute a transformation matrix  $\mathbf{M}$ , consisting of a translation and scaling, that takes points  $\mathbf{p}_k$  to a new set of points  $\tilde{\mathbf{p}}_k$  such that the centroid of the points  $\tilde{\mathbf{p}}_k$  is the coordinate origin  $(0,0)^T$ , and their average distance from the origin is  $\sqrt{2}$ .

(ii) **Normalisation of  $\mathbf{p}'$ :** Compute a similar transformation matrix  $\mathbf{M}'$ , transforming points  $\mathbf{p}'_k$  to  $\tilde{\mathbf{p}}'_k$ .

(iii) **Estimate homography:** Estimate the homography matrix  $\tilde{\mathbf{H}}$  from the normalised correspondences  $\tilde{\mathbf{p}}_k \rightarrow \tilde{\mathbf{p}}'_k$  using the algorithm described earlier in the main section.

(iv) **Denormalisation:** The final homography matrix is given by:

$$\mathbf{H} = \mathbf{M}'^{-1} \tilde{\mathbf{H}} \mathbf{M}.$$

## 4 THE CORRECTION SCHEME

Fig. 2 shows the block schematic of the correction scheme. At MRT, the full declination range for each sidereal hour range is divided into 4 *zones* (refer *second row* in Fig. 1a or 1b). Each zone is imaged with different delay settings to keep the bandwidth decorrelation to  $< 20\%$ . Therefore, the 6 sidereal hours of images under consideration, have 24 images ( $\sim 15^\circ \times 15^\circ$ ).

Using the population of common sources, there are four possible alternatives to correct MRT images by computing:

- (i) 24 homography matrices - one for each image.
- (ii) 6 matrices - one for each sidereal hour.
- (iii) 4 matrices - one for each declination zone.
- (iv) A single homography matrix for the entire steradian.

In principle, bright sources in each image ( $15^\circ \times 15^\circ$ ) can be used to independently estimate a homography matrix. Our earlier experiments to correct each image independently showed that the homography matrices were similar. The plots of errors in  $\alpha$  and  $\delta$  plotted against  $\alpha$  and  $\sin za$  (refer to Fig. 1a and 1b) indicate that the errors are independent of the four delay zones and the range of  $\alpha$ . This implies that estimating a single homography matrix for the entire source population should suffice in representing the errors.

The homography matrix estimated using  $\sim 400$  common sources (described in Section 2) is:

$$\mathbf{H} = \begin{bmatrix} 1.0000 & 0.0006 & 0.0001 \\ 0.0000 & 0.9990 & -0.0009 \\ 0.0000 & 0.0000 & 1.0000 \end{bmatrix}. \quad (5)$$

In the estimated homography matrix,  $h_{11} = 1.0000$  indicates there is no correction required in  $\alpha$  as a function of  $\alpha$ .  $h_{12} = 0.0006$  indicates MRT images should be corrected in  $\alpha$  with a

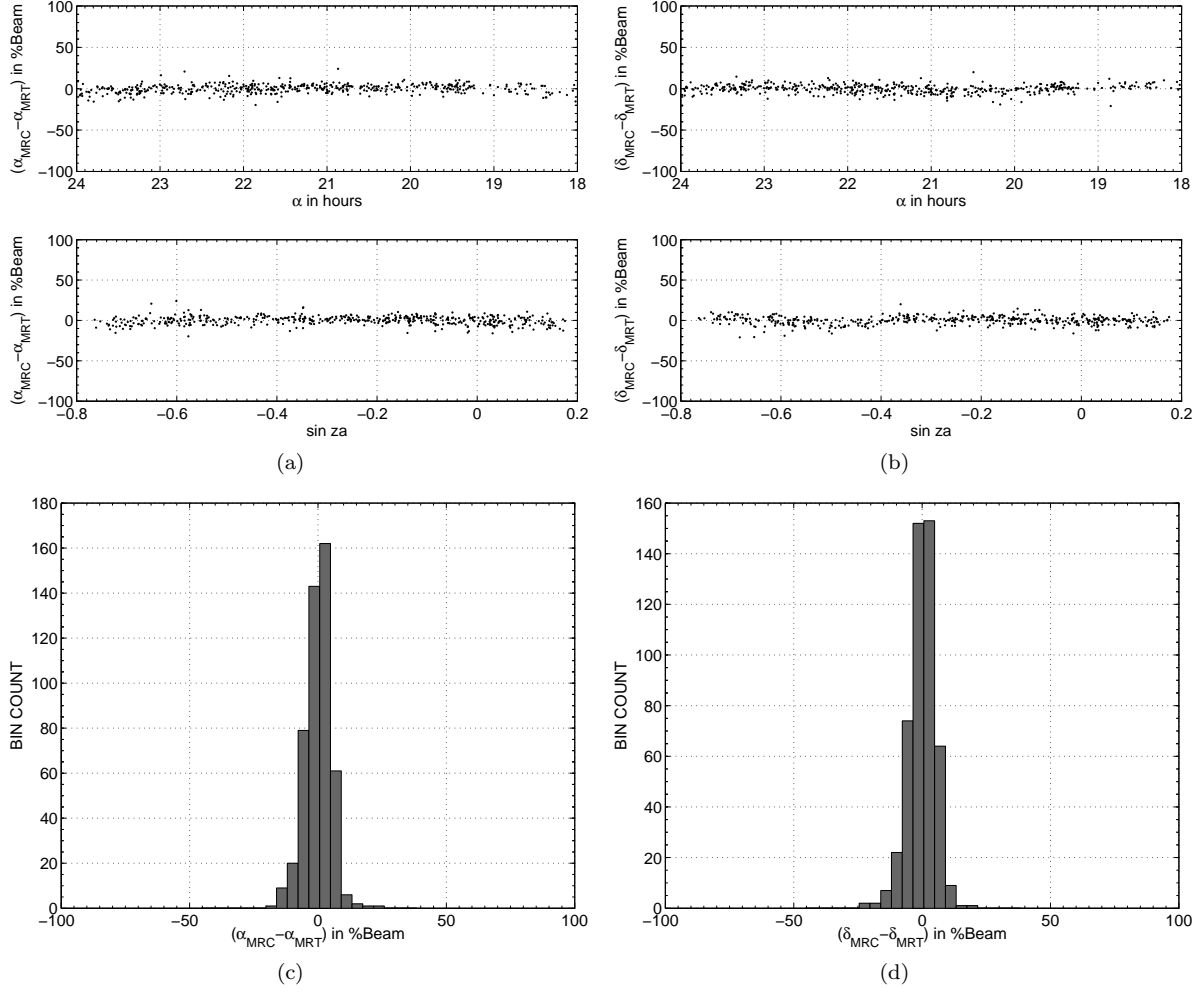


**Figure 3.** Positional error analysis after homography-based correction. (a) *First* and *second* row subplots show errors in  $\alpha$  against  $\alpha$  and  $\sin za$ , respectively. (b) The *first* and *second* row subplots show errors in  $\delta$  against  $\alpha$  and  $\sin za$ , respectively. (c) and (d) show histograms of errors in  $\alpha$  and  $\delta$ , respectively. A comparison of these plots with Fig. 1 demonstrate that homography has removed the systematics and the residual errors are within 10% of the beamwidth.

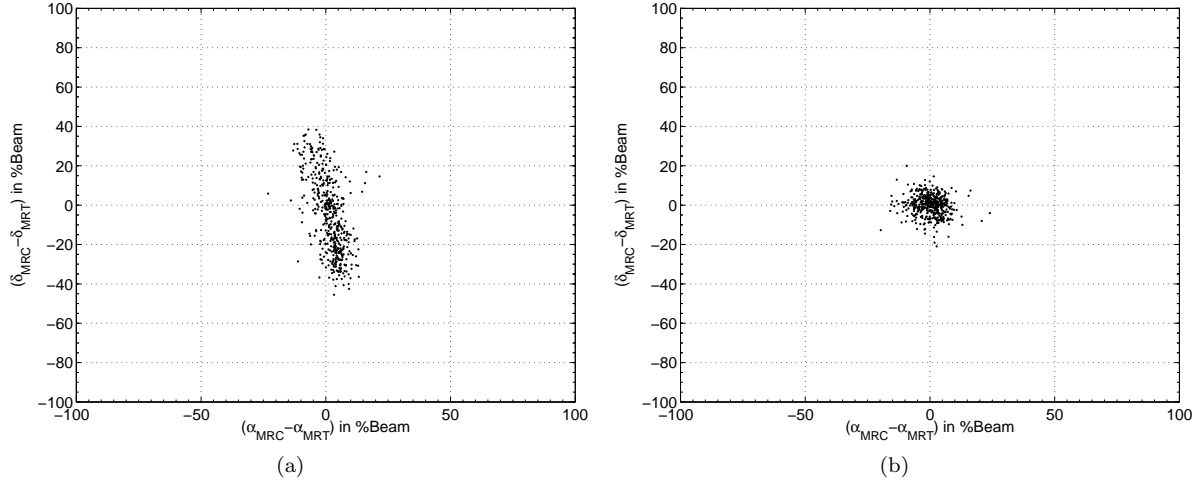


**Figure 4.** Scatter plot of errors in  $\alpha$  and  $\delta$ . (a) Before correction and (b) after homography-based correction. After correction the scatter is almost circular as opposed to elliptical before correction. The rms before correction is  $\sim 20\%$  of the beamwidth. After correction, the rms is reduced to  $\sim 7\%$  of the beamwidth and, the systematic errors have been removed.

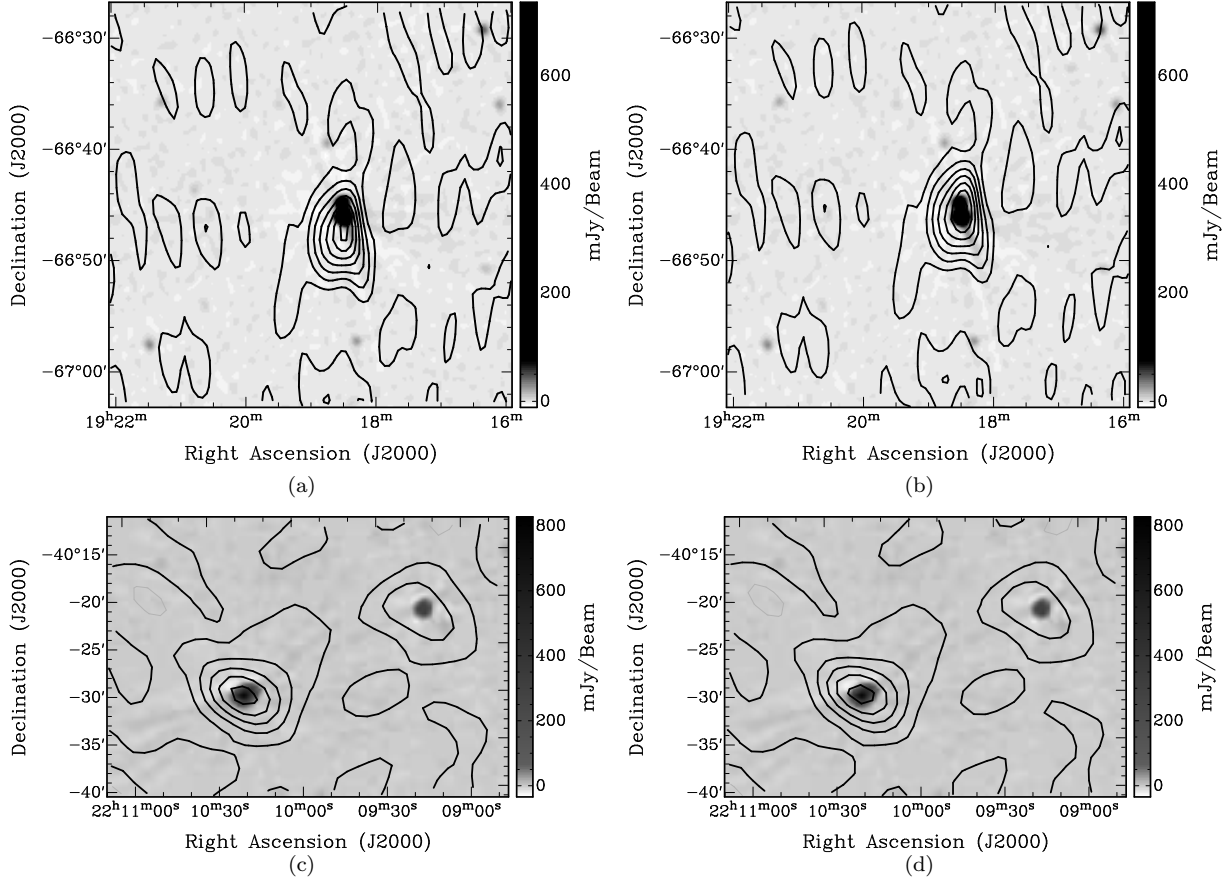


**Figure 5.** MRT contours overlaid on SUMSS image. (a) and (c) MRT contours before correction for sources at about  $\delta = -66^\circ$  and  $\delta = -40^\circ$ , respectively. (b) and (d) Corresponding MRT contours after homography-based correction show that 2-D homography corrected the positional errors. Notice, (c) and (d) are included here for visual emphasis. Since the errors around  $\delta = -40^\circ$  are within 10% of the beamwidth the contours show a good overlap both before and after and, as expected homography has not applied perceivable correction to images at this declination.

$\sin \alpha$  dependence. The estimated correction is up to  $\sim 10\%$  of the beam in  $\alpha$ , at the extreme ends of the  $\sin \alpha$  range. Similarly,  $h_{21} = 0.0000$  indicates that there is no correction required in  $\sin \alpha$ , as a function of  $\alpha$ . However,  $h_{22} = 0.9990$  indicates that MRT images should be compressed in  $\sin \alpha$  by a factor of 0.9990 (which is  $\sim 1$  part in 1000). The values of  $h_{13}$  and  $h_{23}$  indicate that the zero cross-overs of errors in both  $\alpha$  and  $\sin \alpha$  plotted against  $\sin \alpha$  are close to the  $\sin \alpha$  of the calibration source (MRC 1932-464) used for imaging.

Using Equation 1, the homography matrix is used to project each pixel from the images to a new position, effectively correcting for positional errors in images.

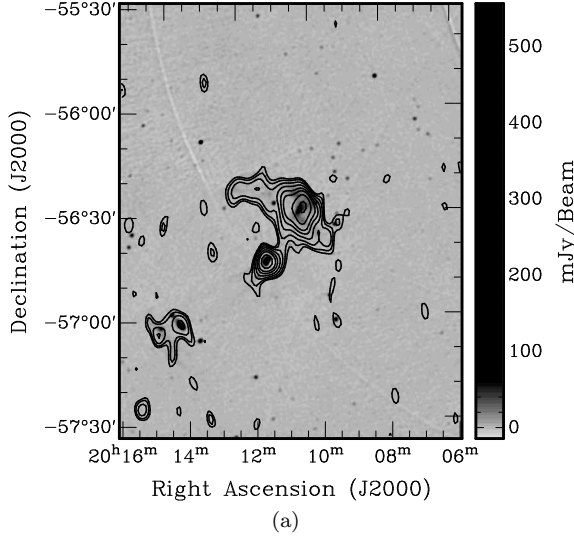
#### 4.1 Corrected images and discussion

Fig. 3 shows positional errors in  $\delta$  after homography-based correction. A comparison of these plots with Fig. 1 demonstrate that homography has removed the systematics and the residual errors are within 10% of the beamwidth for sources above  $15\text{-}\sigma$ , as expected. Fig. 4a and Fig. 4b show scatter plots of errors in  $\delta$  against errors in  $\alpha$  before and after correction, respectively. For visualisation, the errors are represented in percentages of respective MRT beamwidths. Notice, after correction (refer Fig. 4b) the scatter is al-

most circular as opposed to elliptical before correction (refer Fig. 4a). The rms before correction is  $\sim 20\%$  of the beamwidth. After correction, the rms is reduced to  $\sim 7\%$  of the beamwidth and, the systematic errors have been removed.

Fig. 5a and 5b show MRT contours before and after correction, respectively, overlaid on SUMSS (Sydney University Molonglo Sky Survey) image (Mauch et al. 2003), for a source around  $\delta = -67^\circ$ . The corrected MRT image contours in Fig. 5b overlap with the source in SUMSS image. Figs. 5c and 5d show similar comparison for a source around  $\delta = -40^\circ$ . Notice Fig. 1d, since the errors around  $\delta = -40^\circ$  are within 10% of the beamwidth, the contours in both Figs. 5c and 5d show a good overlap as expected and homography has not applied perceivable correction to images at this declination. We have overlaid MRT contours on a number of extended sources at 843 MHz reported by Jones and McAdam (1992). Fig. 6 shows a typical overlay of MRT contours on SUMSS image of a region around the cluster Abell 3667. The overlay is perceptively satisfactory.

The 2-D homography corrected the positional errors in the image domain. For imaging the remaining  $\sim 3.5$  steradians of MRT survey,  $\sim 15000$  hours of data has to be reduced. Ideally, for imaging the new regions, one would like to trace



**Figure 6.** MRT contours overlaid on SUMSS image of a region around Abell 3667.

the source of these errors and correct them in the visibilities. In the following section we discuss how we traced the source of errors and corrected them in the visibility domain.

## 5 ARRAY GEOMETRY: HYPOTHESIS & RE-ESTIMATION

This section describes our *expansion-compression* hypothesis for the source of errors in our images. The subsequent corrections we estimated and applied to eliminate the errors are also described.

For meridian transit imaging,  $m = \sin za$ . The brightness distribution in the sky as a function of  $\sin za$  and the complex visibilities measured for different values of the north-south (NS) baseline vector component  $v$  form a Fourier pair (Christiansen and Högbom 1985). A scaling error of  $\kappa$  in  $m$  will result in a scaling factor of  $\kappa^{-1}$  in the  $v$ -component of the baseline vector. By positional error analysis it is clear that MRT images are stretched (*expanded*) in declination, i.e.,

$$m_{\text{imaged}} = \kappa m_{\text{true}} \quad (6a)$$

$$\therefore v_{\text{measured}} = \kappa^{-1} v_{\text{true}}. \quad (6b)$$

Note, for images the 2-D homography estimated a correction (*compression*) factor,  $\kappa^{-1}$ , of 0.9990. This cued to the hypothesis that we have compressed the north-south baseline vectors. Equation 6b means, a baseline distance of  $\sim 1000$  m in the NS arm was wrongly measured as  $\sim 999$  m (1 part in 1000). Similarly, a  $\sin za$ -dependent correction in  $\alpha$  cued to possible  $v$ -component in the east-west (EW) baseline vectors. Next, we describe the re-estimation of array geometry.

We begin with a brief description of the mode of observations with MRT. MRT has 32 fixed antennas in the EW arm and 15 movable antenna trolleys in the NS arm. For measuring visibilities, the 15 NS trolleys are configured by spreading them over 84 m with an inter-trolley spacing of

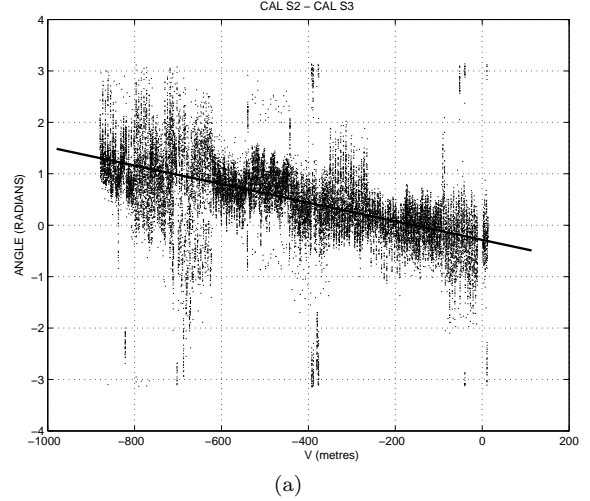


**Figure 7.** Typical calibrator phase differences (in radians) of MRC0915-118 & MRC1932-464, plotted against  $v$  (in metres). The straight line shown is a linear robust fit obtained for the data.

6 m (to avoid shadowing of one trolley by another). MRT measures different Fourier components of the brightness distribution of the sky in 63 different configurations (referred to as *allocations*) to sample NS baselines every 1 m. Therefore, effectively, there are 945 antenna positions (63 allocations \* 15 antennas/allocation) in the NS arm and a total of 30,240 (945 \* 32) visibilities are used for imaging.

A small error in a measuring scale of relatively shorter length is likely to build up systematically while establishing the geometry of longer baselines. This effect would be observed in the instrumental phases estimated using different calibrators. In principle, the instrumental phases estimated using two calibrators at different declinations, for a given baseline, should be the same, allowing for temporal variations in the instrumental gains. A non-zero difference in these estimates may be due to positional errors of the baseline or positions of calibrators. As mentioned earlier, our analysis of positional error in sources and the homography matrix cued to positional errors in baselines (or antenna positions). The simple principle of astrometry (Thomson et al. 2001) was used to estimate errors in antenna positions and is discussed below.

The observed visibility phase,  $\psi_{ij}^{S_1}$ , in a baseline with components  $(u_{ij}, v_{ij}, w_{ij})$ , due to calibrator  $S_1$  with direction cosines  $(l^{S_1}, m^{S_1}, n^{S_1})$ , is given by:

$$\psi_{ij}^{S_1} = l^{S_1} u_{ij} + m^{S_1} v_{ij} + n^{S_1} w_{ij} + \phi_{ij}^{\text{ins}}. \quad (7)$$

Where,  $\phi_{ij}^{\text{ins}}$  represents true instrumental phases,  $i = 1, 2, \dots, 32$  represents EW antennas and  $j = 1, 2, \dots, 945$  represents NS antennas. For meridian transit imaging Equation 7 becomes:

$$\psi_{ij}^{S_1} = -v_{ij} \sin(ZA^{S_1}) + w_{ij} \cos(ZA^{S_1}) + \phi_{ij}^{\text{ins}}. \quad (8)$$

The instrumental phases,  $\phi_{ij}^{S_1}$ , estimated using the measured geometry are given by:

$$\phi_{ij}^{S_1} = -\Delta v_{ij} \sin(ZA^{S_1}) + \Delta w_{ij} \cos(ZA^{S_1}) + \phi_{ij}^{\text{ins}}. \quad (9)$$

Here,  $\Delta v_{ij}$  and  $\Delta w_{ij}$  are errors in the assumed baseline

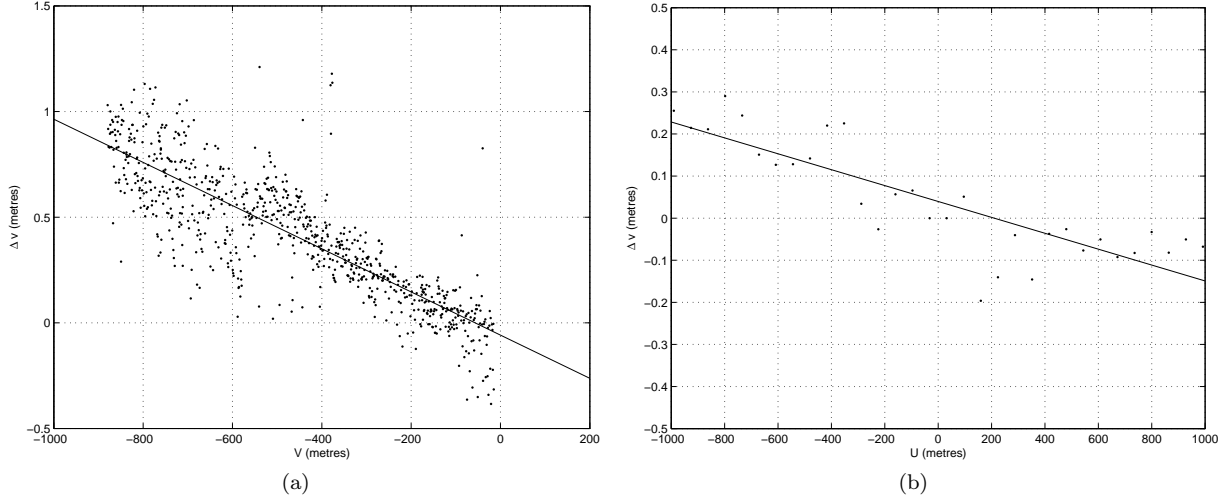


**Figure 8.** (a) Estimate of the antenna position along the North-South arm of MRT array. The fit to the estimates shows a gradient of 1 part in 1000, along the north-south. (b) Estimate of the error in  $v$  coordinate of MRT east-west arm. The fit to the estimate shows a gradient of 2 part in 10,000, along the east-west.

vectors.  $\phi_{ij}^{S_1}$  are phases of complex baseline gains obtained in the process of calibration. Equation 9 has three unknowns. To reduce the number of unknowns, one can eliminate the true instrumental phases by taking a difference ( $\Delta\phi_{ij}^{S_{12}} = \phi_{ij}^{S_1} - \phi_{ij}^{S_2}$ ) between the instrumental phases estimated using two calibrators. This difference gives:

$$\Delta\phi_{ij}^{S_{12}} = -\Delta v_{ij} \left[ \sin(ZA^{S_1}) - \sin(ZA^{S_2}) \right] + \Delta w_{ij} \left[ \cos(ZA^{S_1}) - \cos(ZA^{S_2}) \right]. \quad (10)$$

Note, the  $w$ -components of the baseline vectors are short and non-cumulative measurements. Therefore, in principle, one can consider  $\Delta w_{ij}$  as zero-mean random errors with no systematics. Equation 10 in that case can be written as:

$$\Delta\phi_{ij}^{S_{12}} = -\Delta v_{ij} \left[ \sin(ZA^{S_1}) - \sin(ZA^{S_2}) \right]. \quad (11)$$

Describing the system in terms of errors in antenna positions, as opposed to errors in baseline positions, Equation 11 becomes:

$$\Delta\phi_{ij}^{S_{12}} = -(\Delta v_i - \Delta v_j) \left[ \sin(ZA^{S_1}) - \sin(ZA^{S_2}) \right]. \quad (12)$$

This equation is also not sufficient to solve for errors in the antenna positions as we have two unknowns and one equation. We set up another equation using a third calibrator source,  $S_3$ , spaced away in declination from  $S_1$  and  $S_2$ :

$$\Delta\phi_{ij}^{S_{23}} = -(\Delta v_i - \Delta v_j) \left[ \sin(ZA^{S_2}) - \sin(ZA^{S_3}) \right]. \quad (13)$$

The Equations 12 and 13 are a linear set of equations for one baseline. For the measurements in 63 allocations, the set of equations can be formulated in a matrix form and solved by SVD-based least-squares estimator:

$$\mathbf{Ax} = \mathbf{b}. \quad (14)$$

Where, the *measurement vector*  $\mathbf{x} \in \mathbb{R}^c$  is to be determined. Here,  $c = 977$ . The measurement vector gives  $\Delta v_i$  and  $\Delta v_j$  estimates for 32 EW and 945 NS antenna locations, respectively. The *observation vector*  $\mathbf{b}$  consists of two sub-matrices,

$\mathbf{b}_1 \in \mathbb{R}^{r_1}$  and  $\mathbf{b}_2 \in \mathbb{R}^{r_2}$ , formed using the left-hand-side of Equations 12 and 13, respectively. Here,  $r_1 = r_2 = 30240$ , i.e., the total number of visibilities measured for imaging. Therefore,  $\mathbf{b} \in \mathbb{R}^{60480}$ . The *data matrix*  $\mathbf{A} \in \mathbb{R}^{60480 \times 977}$ . Each row in the data matrix has only two non-zero elements, corresponding to a baseline formed by one EW and one NS antenna, making it very sparse.

The observation vector is constructed from the gain tables of the array obtained using calibrators MRC 0407-658 ( $S_1$ ), MRC 0915-118 ( $S_2$ ) and MRC 1932-464 ( $S_3$ ). The sensitivity per baseline at MRT is  $\sim 26$  Jy for a 1 MHz bandwidth and an integration time of one second. It takes  $\sim 10$  minutes of time for sources at  $\delta = -40^\circ$  to transit a  $2^\circ$  primary beamwidth of elements in the east-west array. This leads to a sensitivity per baseline (including the non-uniform weighting due to primary beam) of  $\sim 2$  Jy. The flux density of these three calibrators as seen by MRT is  $\sim 100$  Jy; strong to get reliable calibration. Further, the calibrators are unresolved and isolated from confusing sources and have well known measured positions (Golap 1998).

A plot of typical phase differences obtained using the pair of calibrators  $S_2$  and  $S_3$  is shown in Fig. 7. Fig. 8a shows the estimated errors in 945 NS antenna positions. The errors show a gradient of 1 part in 1000 along the NS arm. This matches with the linear gradients in the phase differences estimated from the calibrators. The estimates in Fig. 8b show alignment errors of the 32 antennas in the EW arm along the NS-direction. The fit shows a gradient of about 2 part in 10,000. This indicates that the EW arm is mis-aligned from the true EW-direction. At one extreme end (1 km from the centre of the array) of the EW arm the error is  $\sim 0.2$  m, equivalent to an angular distance of  $\sim 40''$  from the centre of the array. This is the source of a small  $\sin \alpha$ -dependent error in  $\alpha$  that was observed in both positional error analysis and the homography matrix. Further, our simulation of the synthesised beam in  $\alpha$  with old EW antenna positions and the corrected EW antenna positions indeed confirm this  $\sin \alpha$ -dependent error in  $\alpha$ .

Using the new antenna positions we have re-imaged one



hour from the steradian and have also imaged a completely new steradian. We find no systematics in positional errors thus endorsing our re-estimated array geometry.

## 6 CONCLUSIONS

The homography-based correction was able to correct for systematics in positional errors in the image domain and the errors are within 10% of the beamwidth for sources above  $15\sigma$ . The corrected images of one steradian are available for download at <http://www.rrr.res.in/surveys/MRT>.

Positional error analysis showed that uncorrected MRT images are stretched in declination by  $\sim 1$  part in 1000. This translates to a compression of the NS baseline vector, in the visibility domain. The analysis also showed a  $\sin \alpha$ -dependent error in  $\alpha$ . This cued towards possible errors in our estimation of the array geometry. By formulating a linear system, using instrumental phases estimated from three well separated calibrators whose positions are well known, the array geometry was re-estimated. The estimated error in the  $v$ -component of the NS baseline vectors is about 1 mm/m. In other words, the error is about half a wavelength at 150 MHz (1 m) for a 1 km baseline. The estimates also show a small (2 part in 10,000)  $v$ -component in the purely EW baseline vectors. This indicates that the EW arm is mis-aligned and inclined at an angle of  $\sim 40''$ , to the true EW direction. These estimates match with the observed stretching of MRT images shown by both the positional error analysis and the homography matrix.

Using the new antenna positions we have re-imaged one hour from the steradian and have also imaged a completely new steradian. We find no systematics in positional errors. This endorses our re-estimated array geometry. Re-imaging one steradian starting from visibilities would have been a very time consuming exercise. Development of 2-D homography-based correction enabled us to correct for the positional errors in the image domain. In our view, this new technique will be of relevance to the new generation radio telescopes where, owing to huge data rates, only images after a certain integration would be recorded as opposed to raw visibilities.

## ACKNOWLEDGEMENT

Soobash Daiboo acknowledges a PhD bursary from the South African Square Kilometer Array project. The authors would like to thank the anonymous referee for the constructive comments and suggestions.

## REFERENCES

- Baldwin J.E., Boysen R.C., Hales S.E.G., Jennings J.E., Waggett P.C., Warner P.J. and Wilson D.M.A., 1985, MNRAS, 217, p717.
- Christiansen W.N. and Högbom J.A., 1985, Radio Telescopes, Cambridge University Press, Second edition.
- Golap K., Issur N.H., Somanah R., Dodson R., Modgekar M., Sachdev S., Udaya Shankar N. and Sastry Ch.V., 1995, J. Astrophys. Astr., 16, p447.
- Golap K., 1998, PhD thesis, University of Mauritius.

- Hartley R.I., 1997, IEEE Tran. on PAMI, 19(6), p580.
- Hartley R.I. and Zisserman A., 2003, Multiple View Geometry in Computer Vision, Cambridge University Press, Second edition.
- Jones P.A. and McAdam W.B., 1992, The Astrophysical Journal Supplement Series, 80, p137.
- Large M.I., Mills B.Y., Little A.G., Crawford D.F., and Sutton J.M., 1981, MNRAS, 194, p693.
- Lonsdale C.J. et. al., 2009, Proceedings of the IEEE, 97, p1497.
- Mauch T., Murphy T., Buttery H.J., Curran J., Hunstead R.W., Piestrzynska B., Robertson J.G. and Sadler E.M., 2003, MNRAS, 342, p1117.
- Pandey V.N. and Udaya Shankar N., 2005, URSIGA.
- Pandey V.N., 2006, PhD thesis, Raman Research Institute.
- Thomson A.R., Moran J.M. and Swenson G.W., 2001, Interferometry and Synthesis in Radio Astronomy, John Wiley & Sons, Second edition.
- Udaya Shankar N., Golap K., Sachdev S., Dodson R., Kataroo M. and Sastry Ch.V., 2002, Ap&SS, 282(1), p15.